Contents

List of Figures

List of Tables

Chapter 1

Introduction and Theory Overview

1.1 Introduction

This thesis presents the analysis details and the results of the search for heavy resonances decaying into a Z boson and a Higgs boson (h) at the center-of-mass energy of 8 TeV, using 19.7 fb^{-1} p-p collision data. In turn, the Z boson is identified through its leptonic decays (leptons often refer to e and μ only in experiments. $l = e, \mu$). The Higgs boson h is expected to hadronically decay into a pair of b-quarks. The investigated final states consist of two charged leptons which are identified in the detector and limit the presence of the background, and two b-quarks from the hadronic Higgs decay which collects the largest possible fraction of Higgs events.

This thesis is organised as follows. In the latter part of this chapter, the model that predicts heavy resonances is introduced, including the expected cross section and the specification of model parameters. In chapter 2, the LHC and the CMS experiment are described, including the information of each sub-detector and the trigger system of the CMS. The details of the analysis are shown in chapter 3. This chapter reveals the way to reconstruct physical objects in CMS. By adding some proper kinematic selections on those physics objects, the interested events in data collected by the CMS detector can be selected. Moreover, this chapter shows the comparison between data and simulation. In the last chapter, the results of the search and the conclusion are presented.

1.2 Theory Overview

Although the Higgs boson discovered by the ATLAS and CMS collaborations [1–3] imposes strong constraints on theories beyond the Standard Model(SM), the extreme fine tuning in quantum corrections required to have a light fundamental Higgs boson with mass close to 125 GeV [4–7] suggests that the Standard Model may be incomplete, and not valid beyond a scale of a few TeV. Various dynamical electroweak symmetry breaking scenarios which attempt to solve this naturalness problem, such as Minimal Walking Technicolor [8], Little Higgs [9–11], or composite Higgs models [12–14] predict the existence of new resonances decaying to a vector boson plus a Higgs boson.

1.2.1 Heavy Vector Triplet Model

Resonance searches are typically not sensitive to all the details and the free parameters of the underlying model, but only to those parameters or combinations of parameters that control the mass of the resonance and the interactions involved in its production and decay. Therefore, one can employ a simplified description of the resonance defined by a phenomenological Lagrangian where only the relevant couplings and mass parameters are retained. This model-independent strategy applies a Heavy Vector Triplet (HVT) [15] to the Standard Model group and reproduces a large class of explicit models. In Eq. (1.1), the mathematical form of the simplified Lagrangian is defined, where V_ν^a , $a = 1,2,3$, is a real vector with vanishing hypercharge in the adjoint representation of $SU(2)_L$, it decscribes one charged and one neutral heavy spin-1 particle with charge eigenstate fields, and $D_{[\mu} V_{\nu]}^a$ represents the covariant derivative.

$$\mathcal{L}_V = -\frac{1}{4} D_{[\mu} V_{\nu]}^a D^{[\mu} V^{\nu]a} + \frac{m_V^2}{2} V_\mu^a V^{\mu a}$$
$$+ i g_V c_H V_\mu^a H^\dagger \tau^a \overset{\leftrightarrow}{D}{}^\mu H + \frac{g^2}{g_V} c_F V_\mu^a \sum_f \bar{f}_L \gamma^\mu \tau^a f_L$$
$$+ \frac{g_V}{2} c_{VVV} \epsilon_{abc} V_\mu^a V_\nu^b D^{[\mu} V^{\nu]c} + \text{quadrilinear terms} \tag{1.1}$$

$$V_\mu^\pm = \frac{V_\mu^1 \mp iV_\mu^2}{\sqrt{2}} \; , \; V_\mu^0 = V_\mu^3 \tag{1.2}$$

$$D_{[\mu} V_{\nu]}^a = D_\mu V_\nu^a - D_\nu V_\mu^a \; , \; D_\mu V_\nu^a = \partial_\mu V_\nu^a + g\epsilon^{abc} W_\mu^b V_\nu^c \tag{1.3}$$

$$H = \begin{pmatrix} \phi^+ \\ \phi^- \end{pmatrix} = \begin{pmatrix} \frac{1}{\sqrt{2}}(\phi_1 + i\phi_2) \\ \frac{1}{\sqrt{2}}(\phi_3 + i\phi_4) \end{pmatrix} \tag{1.4}$$

In these models, new heavy vector bosons $(V^\pm, V^0)$ that couple to the SM Higgs doublet (Eq. 1.4) and SM gauge bosons with the parameters c_H and g_V and to the fermions via the combination $(g^2/g_V)c_F$. The parameter g_V represents the strength of the new vector boson interaction, while c_H and c_F represent the couplings to the Higgs and the fermions respectively, and are expected to be of the order of unity in most models.

1.2.2 Basic Phenomenology

Masses and Mixings

After electro-weak symmetry breaking (EWSB), the only massless state is photon, which can be identified as the gauge field associated with the unbroken $U(1)_{em}$. The two other neutral mass eigenstates are the SM Z boson and one heavy vector of mass M_0 which are obtained by diagonalizing the mass matrix of the (Z, V^0) system by a rotation with angle θ_N

$$\begin{pmatrix} Z \\ V^0 \end{pmatrix} \rightarrow \begin{pmatrix} \cos\theta_N & \sin\theta_N \\ -\sin\theta_N & \cos\theta_N \end{pmatrix} \begin{pmatrix} Z \\ V^0 \end{pmatrix}. \tag{1.5}$$

The mass matrix is

$$
\mathcal{M}_N^2 = \begin{pmatrix} \hat{m}_Z^2 & c_H \xi \hat{m}_Z \hat{m}_V \\ c_H \xi \hat{m}_Z \hat{m}_V & \hat{m}_V^2 \end{pmatrix} \; , \; \text{where} \begin{cases} \hat{m}_Z = \frac{e\hat{v}}{2 \sin\theta_W \cos\theta_W} \\ \hat{m}_V^2 = m_V^2 + g_V^2 c_{VVHH} \hat{v}^2 \\ \xi = \frac{g_V \hat{v}}{2\hat{m}_V} \end{cases} . \tag{1.6}
$$

In the above equations $\hat{v}$ denotes the Vacuum Expetation Value (VEV) defined by $\langle H^\dagger H \rangle = \hat{v}^2/2$, and one should know the masses $\hat{m}_Z$ and $\hat{m}_V$ do not coincide with the physical Z boson and the masses of the new resonances of this model, although they do in the approximations later. The mass eigenvalues and the rotation angles are easily obtained by inverting the relations

$$
Tr[\mathcal{M}_N^2] = \hat{m}_Z^2 + \hat{m}_V^2 = m_Z^2 + M_0^2 \; ,
$$
$$
Det[\mathcal{M}_N^2] = \hat{m}_Z^2 \hat{m}_V^2 (1 - c_H^2 \xi^2) = m_Z^2 M_0^2 \; ,
$$
$$
\tan 2\theta_N = \frac{2c_H \xi \hat{m}_Z \hat{m}_V}{\hat{m}_V^2 - \hat{m}_Z^2} \; . \tag{1.7}
$$

Notice that the tangent can be uniquely inverted because the angle θ_N is in the range $[-\pi/4, \pi/4]$ in the parameter region we will be interested in, where $\hat{m}_Z < \hat{m}_V$, and M_0 represents the real mass eigenvalue of the neutral heavy vector boson.

The situation is similar in the charged vector mass matrix of $(W^\pm, V^\pm)$ system, and $M_\pm$ denotes the real mass eigenvalue of charged states as well.

$$
\mathcal{M}_C^2 = \begin{pmatrix} \hat{m}_W^2 & c_H \xi \hat{m}_W \hat{m}_V \\ c_H \xi \hat{m}_W \hat{m}_V & \hat{m}_V^2 \end{pmatrix} \; , \; \text{where } \hat{m}_W = \frac{e\hat{v}}{2 \sin\theta_W} = \cos\theta_W \hat{m}_Z \; , \tag{1.8}
$$

where it is diagonalized by

$$
Tr[\mathcal{M}_C^2] = \hat{m}_W^2 + \hat{m}_V^2 = m_W^2 + M_\pm^2 \; ,
$$
$$
Det[\mathcal{M}_C^2] = \hat{m}_W^2 \hat{m}_V^2 (1 - c_H^2 \xi^2) = m_W^2 M_\pm^2 \; ,
$$
$$
\tan 2\theta_C = \frac{2c_H \xi \hat{m}_W \hat{m}_V}{\hat{m}_V^2 - \hat{m}_W^2} \; . \tag{1.9}
$$

By checking Eq. (1.6) and Eq. (1.8), the charged and neutral mass matrices are connected by custodial symmetry, which can be shown in full generality to imply

$$\mathcal{M}_C^2 = \begin{pmatrix} \cos\theta_W & 0 \\ 0 & 1 \end{pmatrix} \mathcal{M}_N^2 \begin{pmatrix} \cos\theta_W & 0 \\ 0 & 1 \end{pmatrix} . \tag{1.10}$$

By taking the determinant of the above equation, or equivalently by comparing the charged and neutral determinants in Eq. (1.7) and Eq. (1.9), we obtain a generalized custodial relation among the physical masses

$$m_W^2 M_\pm^2 = \cos^2\theta_W m_Z^2 M_0^2 . \tag{1.11}$$

From the simple formula above, we can start to identify the physically reasonable region of the parameter space in this model. We aim at describing new vectors with masses at or above the TeV scale, but we also want the SM masses $m_{W,Z} \sim 100$ GeV to be reproduced. Therefore we require a hierachy in the mass relation of SM Z and W bosons versus the new vectors.

$$\frac{\hat{m}_{W,Z}}{\hat{m}_V} \sim \frac{m_{W,Z}}{M_{\pm,0}} \leq 10^{-1} \ll 1 \tag{1.12}$$

In the limit of Eq. (1.12) we obtain simple approximation for m_W and m_Z

$$m_Z^2 = \hat{m}_Z^2(1 - c_H^2\xi^2)(1 + \mathcal{O}(\hat{m}_Z^2/\hat{m}_V^2)) ,$$
$$m_W^2 = \hat{m}_W^2(1 - c_H^2\xi^2)(1 + \mathcal{O}(\hat{m}_W^2/\hat{m}_V^2)) . \tag{1.13}$$

The parameter ξ can be either very small or of order unity. Both cases are realized in explicit models. While $\xi \ll 1$ is the most common situation, $\xi \sim 1$ only occurs in strongly coupled scenarios at very large g_V. In these approximations, SM tree-level experimental observation can be reproduced to percent accuracy.

Since $\hat{m}_W = \cos\theta_W \hat{m}_Z$, the W-Z mass ratio is thus given by

$$\frac{m_W^2}{m_Z^2} \simeq \cos^2\theta_W \ . \tag{1.14}$$

Eq. (1.14) has one important implication on the masses of the new vectors. When combined with the custodial relation Eq. (1.11), it tells us that the charged and neutral Vs are practically degenerate

$$M_\pm^2 = M_0^2(1 + \mathcal{O}(\%)) \ , \tag{1.15}$$

In the following, when working at the leading order in the limit Eq. (1.12), we can ignore the mass splitting and denote the mass of the charged and the neutral states collectively as M_V. It is easy to check that in that limit $M_V = \hat{m}_V$.

Decay Widths

Because of the hierachy in the mass matrices, the mixing angles are naturally small. By looking at Eqs. (1.7), (1.9) and (1.12) we can estimate

$$\theta_{N,C} \simeq c_H \xi \frac{\hat{m}_{W,Z}}{\hat{m}_V} \leq 10^{-1} \ , \tag{1.16}$$

and after rotating to the mass basis, the coupling of the neutral and charged resonances to left- and right-handed fermion chiralities can be written in a compact form for each fermion species $F = \{l, q, 3\}$.

$$\begin{cases} g_L^N = \frac{g^2}{g_V} \frac{c_F}{2} \cos\theta_C + (g_L^Z)_{SM} \sin\theta_N \simeq \frac{g^2}{g_V} \frac{c_F}{2} \ , \\ g_R^N = (g_R^Z)_{SM} \sin\theta_N \simeq 0 \\ g_L^C = \frac{g^2}{g_V} \frac{c_F}{2} \cos\theta_C + (g_L^W)_{SM} \sin\theta_C \simeq \frac{g^2}{g_V} \frac{c_F}{2} \ , \\ g_R^C = 0 \end{cases} \tag{1.17}$$

In the above equation $(g^{W,Z}_{L,R})_{SM}$ denote the ordinary SM W and Z couplings (with the normalization given by $g^W_L = g/\sqrt{2}$).

Given that the rotation angles are small, the couplings further simplify, as also shown in the equation. We could see that V interact mainly with left-handed chiralities and that all the couplings for each fermion species are controlled by the parameter combination $g^2/g_V c_F$. This gives tight correlations among different channels

$$\Gamma_{V_\pm \to f\bar{f}'} \simeq 2\Gamma_{V_0 \to f\bar{f}'} \simeq N_C[f](\frac{g^2 c_F}{g_V})^2 \frac{M_V}{48\pi} \ , \tag{1.18}$$

where $N_C[f]$ is the number of colors (3 for the di-quark and 1 for the dilepton decays). The parameters $c_F = \{c_l, c_q, c_3\}$ control the relative BRs to leptons, light quarks and the third family.

In the case of di-boson decay width

$$\Gamma_{V_0 \to W^+_L W^-_L} \simeq \Gamma_{V_\pm \to W^\pm_L Z_L} \simeq \frac{g^2_V c^2_H M_V}{192\pi} \frac{(1 + c_H c_{VVV}\xi^2)^2}{(1 - c^2_H \xi^2)^2} = \frac{g^2_V c^2_H M_V}{192\pi}[1 + \mathcal{O}(\xi^2)] \ ,$$

$$\Gamma_{V_0 \to Z_L h} \simeq \Gamma_{V_\pm \to W^\pm_L h} \simeq \frac{g^2_V c^2_H M_V}{192\pi} \frac{(1 - 4c_{VVHH}\xi^2)^2}{1 - c^2_H \xi^2} = \frac{g^2_V c^2_H M_V}{192\pi}[1 + \mathcal{O}(\xi^2)] \ .$$

$$\tag{1.19}$$

Note that Eq. (1.19) is derived in the Equivalent Gauge [16] because the decay to transverse SM vectors is highly suppressed while to the longitudinal parts grows with the energy of the process, therefore the Unitary Gauge which is used in the original Lagrangian is instead useful. The channels that are not shown in the above equations are either forbidden or suppressed like the decays to transverse polarizations. From this section, a very simple picture emerges. At small ξ, all the decay widths are fixed with a given resonance mass M_V and the couplings $\{g^2 c_F/g_V, g_V c_H\}$ which control the BRs in all relevant channels. Paremeters c_{VVV}, c_{VVHH} and c_{VVW} are basically irrelevent. Thus, the basic phenomenology of this model is well described by a good approximation.

1.2.3   Explicit Models

Now the general picture is clear, we can get exact values of the widths and BRs from explicit models. Consider two benchmark models, A and B, which correspond to two explicit models describing the heavy vectors in Refs. [17] and [12] respectively. All the c parameters are fixed to specific values in these models and the only free parameters are the resonance mass M_V and coupling g_V. Moreover, model A is inspired by weakly coupled extensions of the SM gauge group while model B is by strongly coupled scenarios of EWSB, $i.e.$ Composite Higgs models, we will consider them in different regions of g_V, relatively small $g_V \leq 3$ and relatively large $g_V \geq 3$.

Figure 1-1 shows the BRs as functions of the mass in model A and B. As expected from the previous discussion and according to Refs. [17], model A predicts

$$c_H = -g^2/g_V^2 \ , \ c_F \simeq 1 \ ,$$
$$|g_V c_H| \simeq g^2 c_F/g_V \simeq g^2/g_V \ . \tag{1.20}$$

Therefore Eq. (1.18) and (1.19) can be determined in the following form for V_0 in model A ($g_V = 1$),

$$\Gamma_{V_0 \to f\bar{f}'} \simeq N_c[f] \frac{g^4 M_V}{96\pi}$$
$$\Gamma_{V_0 \to W^+ W^-} \simeq \Gamma_{V_0 \to Zh} \simeq \frac{g^4 M_V}{192\pi} \ . \tag{1.21}$$

One can easily check either from the plot or the equation, a factor of two difference comparing the BRs between fermions and bosons. Due to the color factor, leptons and quarks also have a difference by a factor of three. Since the c_F term is universal both in A and B. The total width in model A decreases with increasing g_V because of the overall suppresion (g^2/g_V) in Eq. (1.20).

On the contrary, in model B the c_H term is unsuppressed

$$c_H \simeq c_F \simeq 1 \; ,$$

$$g_V c_H \simeq -g_V \; , \; g^2 c_{c_F}/g_{g_V} \simeq g^2/g_V \; . \tag{1.22}$$

Thus the determinate V_0 decay widths for model B $(g_V = 3)$ are

$$\Gamma_{V_0 \to f \bar{f}'} \simeq N_c[f] \frac{g^4 M_V}{342\pi}$$

$$\Gamma_{V_0 \to W^+ W^-} \simeq \Gamma_{V_0 \to Zh} \simeq \frac{3 M_V}{64\pi} \; . \tag{1.23}$$

68 For model B$_{g_V=3}$ the dominant BRs are into di-bosons and the fermionic decays are

69 extremely suppressed. Moreover, the total width increases with increasing g_V since it

70 is dominated by the di-boson width which grows with g_V as expected from Eq. (1.22).

71 This model B is particularly interesting for the present search, since it predicts signal

72 cross sections in order of fb [15] [18] [Fig. 1-2], branching ratios to vector bosons close

73 to unity, and thus being accessible at the LHC. In the latter chapters, the mass eigen-

74 state of the neutral heavy vector boson in model B scenario refers to the Z' particle,
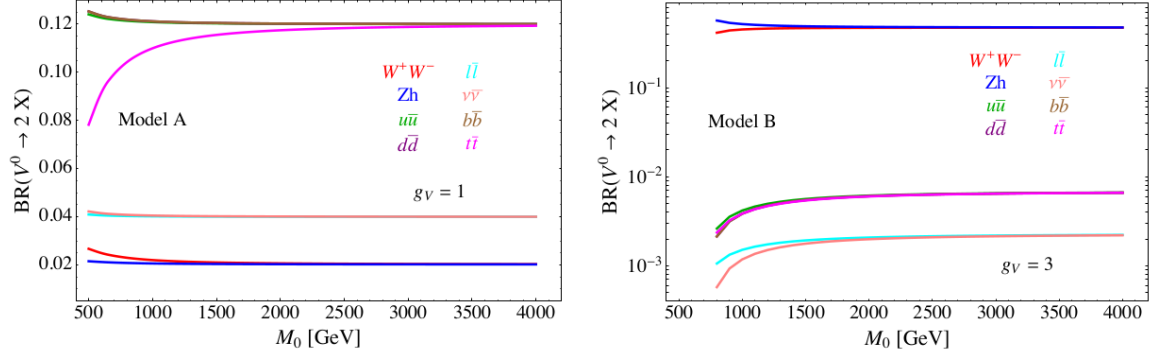
75 which is the search target of this thesis.

76

Figure 1-1: Branching ratios as a function of the resonance mass for the HVT benchmark model A(left) and model B(right).
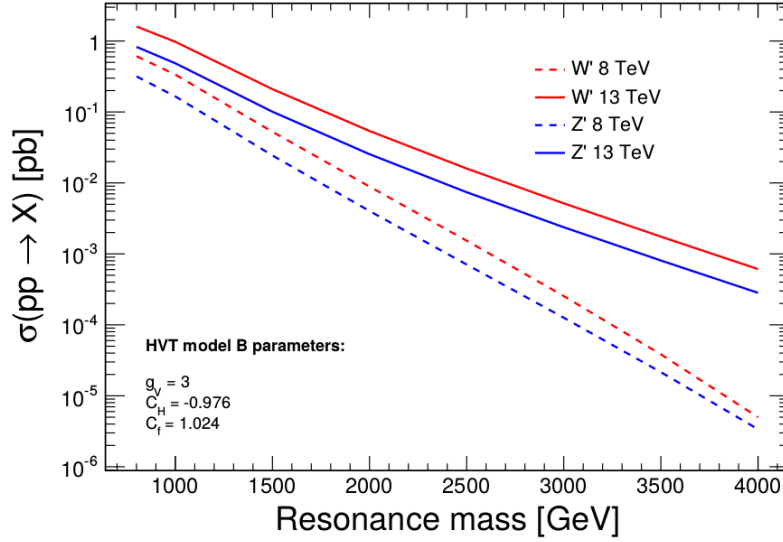

Figure 1-2: Theoretical production cross-section as a function of new resonance particles for the HVT model B benchmark. Dash lines are 8 TeV predictions while solid lines are 13 TeV predictions.

Chapter 2

CMS detector and LHC

This thesis is done via analyzing the data collected by the Compact Muon Solenid (CMS) detector at the Large Hadron Collider (LHC). CMS is one of the two largest detectors built on the LHC. This chapter will briefly introduce the LHC and the CMS detector.

2.1 Large Hadron Collider

The LHC is the world's most powerful hadron collider and the largest experimental facility ever. It was built by the European Organization for Nuclear Research (CERN) between 1998 and 2008 in collaboration with over 10,000 scientists and engineers from over 100 countries, as well as hundreds of universities and laboratories. It lies in a tunnel 27 km in circumference, as deep as 175 m beneath the France−Switzerland border near Geneva. The designed maximum collison energy and highest luminosity of the LHC are 14 TeV and $10^{-34}\text{cm}^{-2}\text{s}^{-1}$ respectively.

Other accelerators that had been originally built at CERN for previous experiments is working as an injection chain for the LHC now. The proton beam starts from LINAC, a small linear accelerator, where its energy firstly reaches 50 MeV. It then passes through a booster and goes to the PS, where it is accelerated up to 25 GeV. After that, it reaches 450 GeV in the SPS. The beam is finally injected in the LHC ring from the SPS, it is accelerated up to 4 TeV in 2012. In early 2015, the proton

beam had been acceletated to 6.5 TeV, a value near its designed energy, before undergoing collision.

There are four collision points at the LHC, corresponding to four main experiments, CMS, ATLAS, LHCb and ALICE. The ALICE experiment is optimized to study heavy-ion (Pb-Pb nuclei) collisions and focusing on the physics of strongly interacting matter at extreme energy densities. LHCb is a specialized b-physics experiment, measuring the parameters of CP violation in the interactions of b-hadrons. Such studies can help to explain the matter-antimatter asymmetry of the universe. Last, CMS and ATLAS are two general purpose detectors. The aims of these two experiments are investigating a wide range of physics, including the search for the beyond standard model particles, extra dimensions, and dark matter.

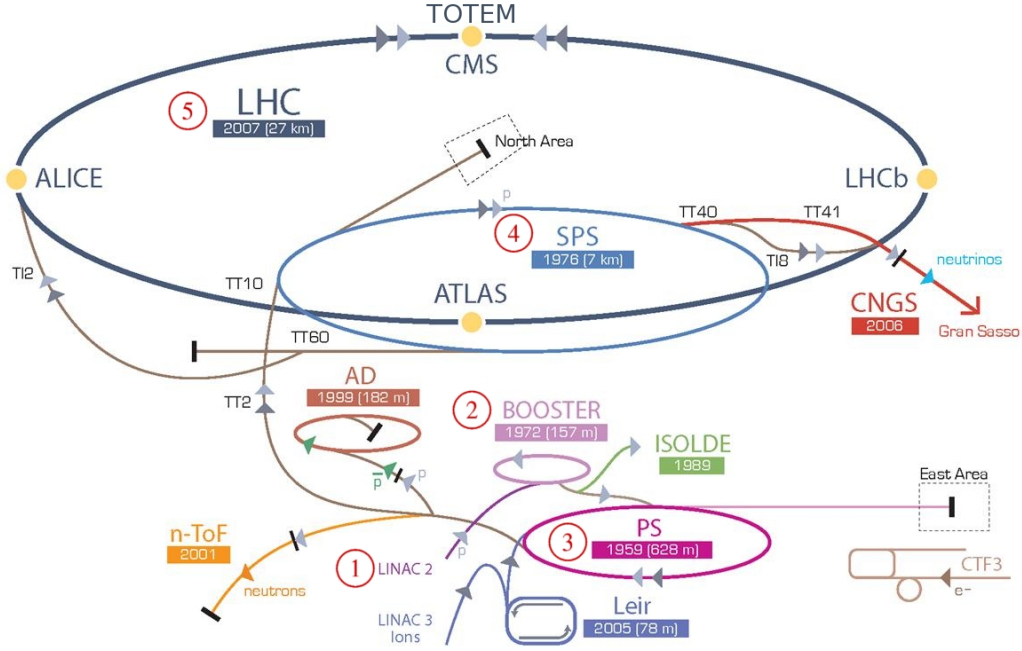Figure 2-1: Overview of the LHC and relative location of the detectors.

Figure 2-2: CERN accelerator complex.

2.2 Compact Muon Solenoid

The Compact Muon Solenoid (CMS) detector is designed to cope very high rate of interactions expected to take place at the high LHC luminosity. It has the typical structure of detectors at hadron colliders: a central region (*barrel*) enclosed by two disks (*endcaps*). The structure of CMS can be seen in Fig. (2-3).

Solenoid and Sub-detectors

CMS features a powerful superconducting coil, generating a solenoidal magnetic field around 3.8 Tesla in a large volume, which hosts different sub-detctors. The magnetic field lines close through steel yoke in the outer region and the distinct sub-detectors are designed in order to obtain the highest possible resolution and the largest acceptance for every kind of particles.

The innermost layer is a silicon-based tracker. Surrounding it is a scintillating crystal electromagnetic calorimeter (ECAL), which is itself surrounded with a sampling

calorimeter for hadrons (HCAL). The tracker and the calorimeters are compact enough to fit inside the CMS Solenoid. Outside the magnet are the large muon detectors separated by layers of the steel yoke.
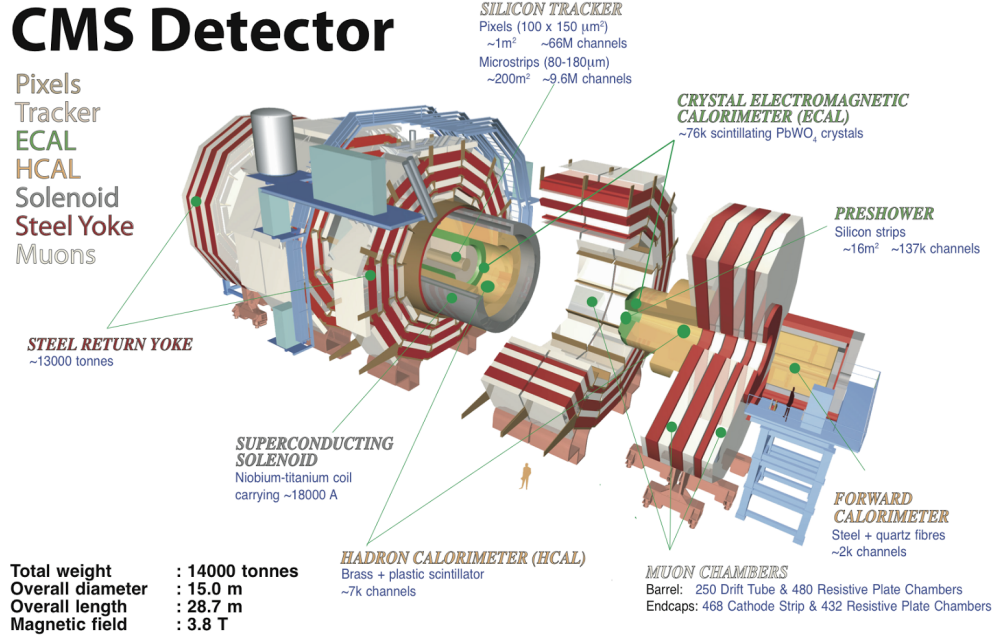

Figure 2-3: Schematic layout of the CMS detector.

Coordinate System

The CMS coordinate system is oriented such that the x-axis points to the center of the LHC ring, the y-axis points vertically upward and the z-axis is in the direction of the beam. The azimuthal angle ϕ is measured from the x-axis in the xy plane and the radial coordinate in this plane is denoted by r. The polar angle θ is defined in the rz plane, while the pseudo-rapidity $\eta = -ln \tan{(\theta/2)}$. The momentum component transverse to the beam direction, denoted by p_T, is computed from the x- and y-components, and the transverse energy is defined as $E_T = E \sin\theta$.

2.2.1   Tracker

2.2.2   ECAL

2.2.3   HCAL

2.2.4   Muon Chamber

2.2.5   Trigger System

Bibliography

[1] ATLAS Collaboration. Observation of a new particle in the search for the Standard Model Higgs boson with the ATLAS detector at the LHC. *Phy. Lett. B*, 716:1, 2012.

[2] CMS Collaboration. Observation of a new boson at a mass of 125 GeV with the CMS experiment at the LHC. *Phy. Lett. B*, 716:30, 2012.

[3] CMS Collaboration. Observation of a new boson with mass near 125 GeV in pp collisions at $\sqrt{s} = 7$ and 8 TeV. *JHEP*, 06:081, 2013.

[4] CMS Collaboration. Precise determination of the mass of the Higgs boson and tests of compatibility of its couplings with the standard model predictions using proton collisions at 7 and 8 TeV. *Eur. Phys. J. C*, 75:212, 2015.

[5] ATLAS Collaboration. Measurement of the Higgs boson mass from the $H \to \gamma\gamma$ and $H \to ZZ^* \to 4l$ channels in pp collisions at center-of-mass energies of 7 and 8 TeV with the ATLAS detector. *Phys. Rev. D*, 90:052004, 2014.

[6] ATLAS Collaboration. Evidence for the spin-0 nature of the Higgs boson using ATLAS data. *Phys. Lett. B*, 726:120, 2013.

[7] CMS and ATLAS Collaboration. Combined Measurement of the Higgs Boson Mass in pp Collisions at $\sqrt{s} = 7$ and 8 TeV with the ATLAS and CMS Experiments. *Phys. Rev. Lett.*, 114:191803, 2015.

[8] Mads T. Frandsen. Minimal Walking Technicolor. arXiv:0710.4333 [hep-ph], http://arxiv.org/abs/0710.4333, 2007.

[9] B. McElrath T. Han, H. E. Logan and L.-T. Wang. Phenomenology of the little Higgs model. *Phys. Rev. D*, 67:095004, 2003.

[10] M. Schmaltz and D. Tucker-Smith. LITTLE HIGGS THEORIES. *Annual Review of Nuclear and Particle Science*, 55:no. 1, 229–270, 2005.

[11] M. Perelstein. Little Higgs models and their phenomenolog. *Progress in Particle and Neclear Physics*, 58:no. 1, 247–291, 2007.

[12] D. Marzocca R. Contino, D. Pappadopulo and R. Rattazzi. On the effect of resonances in composite Higgs phenomenology. *Journal of High Energy Physic*, 2011:no. 10, 1–50, 2011.

[13] M. Serone D. Marzocca and J. Shu. General composite Higgs model. *Journal of High Energy Physics*, 2012:no. 8, 1–52, 2012.

[14] C. Cski B. Bellazzini and J. Serra. Composite Higgses. *Eur. Phys. J.*, C74:no. 5, 2766, 2014.

[15] R. Torre D. Pappadopulo, A. Thamm and A. Wulzer. Heavy vector triplets: bridging theory and data. *Journal of High Energy Physics*, 2014:no. 9, 1–50, 2014.

[16] Andrea Wulzer. An Equivalent Gauge and the Equivalence Theorem. arXiv:1309.6055 [hep-ph], http://arxiv.org/abs/1309.6055, 2013.

[17] W.-Y. Keung V. Barger and E. Ma. Gauge model with light W and Z bosons. *Phys. Rev. D*, 22:727, 1980.

[18] Lisa Benato, Yu-Hsiang Chang, Ching-Wei Chen, Michele de Gruttola, Raman Khurana Ji-Kong Huang, Stefano Lacaprara, Yun-Ju Lu, Jacopo Pazzini, Maurizio Pierini, Henry Yee-Shian Tong, Jun-Yi Wu, Shin-Shan Eiko Yu, Marco Zanetti, and Alberto Zucchetta. Search for heavy resonances decaying into a vector boson and a higgs boson in the $(ll, l\nu, \nu\nu)b\bar{b}$ final state. CMS Note 2015/186, CMS, 2015.